Journal of
Marine Science and Engineering

MDPI

Article

Multiple TLDs on Motion Reduction Control of the Offshore Wind Turbines

Po-Hung Yeh, Shao-Hua Chung and Bang-Fuh Chen *

Department of Marine Environment and Engineering, National Sun Yat-sen University, Kaohsiung 804, Taiwan; kuroshio@mail.nsysu.edu.tw (P.-H.Y.); allen82324@gmail.com (S.-H.C.)

* Correspondence: chenbf@g-mail.nsysu.edu.tw

Received: 26 May 2020; Accepted: 22 June 2020; Published: 24 June 2020

Abstract: This study explores the damping effects of tuned liquid dampers (TLDs) on a monopile offshore wind turbine (OWT). The fluid–solid coupling of ANSYS was used to simulate the damping effect of a TLD on the structures. The environmental conditions refer to the IEC-61400-3 and the Design Load Case (DLC) 1.2 for the annual average environmental conditions and DLC 6.2 for the 50-year regression period, and the extreme environmental conditions were used in the study. The turbulent wind field simulation was performed by TurbSim, and the load of wind waves on structures was generated by FAST, which were all developed by the NREL (National Renewable Energy Laboratory). In addition to wind and waves, the seismic force was also considered. The cylindrical TLD was located above the rotor nacelle assembly (RNA). A TLD has different damping effects when acting under wind, wave, and earthquake loads, respectively. The effect of the TLD regarding motion reduction on the OWT under coupled wind, wave, and seismic loads was studied. This study also designed a simple experiment to verify the correctness of the numerical simulation results. Fatigue analysis shows that multi-layer TLDs can extend the fatigue life (37%) of an OWT. In addition, under extreme environmental load conditions, multi-layer TLDs have a better vibration damping performance than single-layer TLDs. The study demonstrates that multi-layer TLDs can be considered as a vibration reduction damper for OWTs.

Keywords: motion reduction control; renewable energy; TLD; offshore wind turbine

1. Introduction

Although coal is the earliest type of fossil fuel used by human beings, it has always a serious air pollution impact. The nuclear waste treatment and the warm drainage are the major environmental impact issues. Therefore, at present, most countries have started to use renewable energy. Taiwan is an island located in the eastern part of Asia and on the west side of the Pacific Ocean. Taiwan's imported energy accounted for 98.16% of its total energy usage in 2018. It is urgent for the Taiwanese government to develop and increase its renewable energy percentage. Taiwan's northeast monsoon is very strong, especially in the Taiwan Strait. According to the 4C Offshore reported in 2014, the world's 23-year average wind speed observation found that the Taiwan Strait has accounted for 16 places of the world's 20 most windy offshore wind farms. For this reason, the Taiwanese government approved the "Thousand Sea and Land Wind Turbines". The goal is to complete the land wind farm installation with a capacity of 1200 MW. In addition to land farm, the offshore wind farm project is expected to be completed in 2025 with a capacity of 3000 MW and 1000 wind turbines will be installed in the near west coast of Taiwan.

Taiwan is located in the volcanic belt of the Pacific Rim, and it is in the active seismic zone. High seismic activity and frequent typhoon attacks are the threats to offshore structures. Therefore, the offshore structure is usually equipped with a damping device to suppress the vibration of the

structure under extreme loading conditions and reduce the fatigue damage caused by the long-term cyclic loading, thereby prolonging the service life of the offshore structure.

Offshore Wind Turbine (OWT)

Offshore wind turbines are developing rapidly in recent years because the OWTs have higher wind speeds, less noise, and less land occupation than on-land WTs. The OWTs may generate large amounts of energy as the extreme wind and wave loads act on the OWTs, which usually have a slender supported tower and a monopile foundation. Therefore, the damping device is needed to reduce the dynamic response of OWTs. Structural control includes active, semi-active, and passive control, and the passive control is the simplest control method. The tuned mass damper (TMD) is a passive control that absorbs structural vibration by mass swing. For example, the control system of the top floor of Taipei 101 is a tuned mass damper. Murtagh et al. [1] applied TMD to control the vibration of the OWT, and two TMDs were placed in the cabin of OWT to reduce the vibration in the fore-aft and side-to-side directions. Sun and Jahangiri [2] designed a three-dimensional pendulum tuned mass damper (3d-PTMD) to control the multi-directional vibration of the OWT, and it has 10% more damping effect than double TMDs have. Hemmati and Oterkus [3] developed a semi-active TMD for the vibration reduction of OWTs; they used a short-time Fourier transform to adjust the damping system to the instantaneous frequency of the system to achieve a better damping effect. The results showed that the performance of a semi-active TMD with a mass ratio (the ratio of mass of TMD to mass of the structure) of 1% is better than a passive TMD with a mass ratio of 4%. Since the installation and maintenance costs of TMD are quite expensive, in order to reduce the cost, the tuned liquid damper (TLD) has been developed. The sloshing liquid counteracts with the externally applied force to achieve the shock absorption effect. The working principle of TLD is based on sloshing of the liquid to absorb a portion of the dynamic energy of the structure subjected to dynamic loadings and thus controls the structural vibration.

As early as 1950, the TLD has been used to stabilize ships. Modi and Welt [4] used the liquid sloshing in the annular tank to dissipate the sloshing energy and evaluate whether the damper can attenuate the low-frequency vibrations of the structure in aerodynamics, and that damper can effectively suppress the vibration of the structure under wind loads. Fujii et al. [5] developed multi-layer tuned liquid dampers (TLDs), which were used in the Nagasaki Airport Building (42 m high) and the Yokohama Marine Building (101 m high) under strong winds, which can reduce structural vibration by about 50%. Kareem [6] avoids calculating complex free liquid levels by converting the sloshing of the liquid into a particle spring system, and then simulated the effect of TLD installation in high-rise buildings. Sun et al. [7] established a rectangular nonlinear TLD model, using the shallow water wave theory to consider the damping effect and breaking waves of the liquid, and then using fluid–solid coupling to obtain the effect of TLD on the structure. Wakahara et al. [8] studied the optimization of TLD design on high-rise buildings, explored the parameters of changing TLD design, and developed new methods to predict the suppression of high-rise buildings by TLDs. Tamura et al. [9] set up TLDs on buildings to verify the motion reduction effect of the TLD. It turns out that the TLD can significantly improve the durability of the building.

Sakai [10] proposed another TLD-based damping method, tuned liquid column damper (TLCD), which used a U-tube as a container for liquids, and the vibration of the structure is reduced by the sway of the liquid in the tube. Colwell and Basu [11] used a TLCD to reduce the vibration of OWTs under wind and wave loads, and they applied Miner's law in their fatigue analysis. They reported that TLCD can effectively reduce the vibration generated by strong winds and waves, and it can also reduce the fatigue damage caused by wind waves. However, because the OWT is a long and narrow structure, the performance of the TLCD depends on the width of the bottom and the total length proportion. The greater the proportion of the bottom width, the better the shock absorption performance, but the width of the OWT is limited (cannot be large), and the performance of the container is limited as well. On the other hand, the TLCD can only absorb vibration in one direction, but the direction of the wind

and waves on the sea does not necessarily coincide, so the load action on the OWT is not only in one direction. Colwell suggests that it can install multiple sets of TLCDs in different directions or use TLD to achieve multi-directional damping. Jin et al. [12] used a cylindrical TLD to control the vibration of the offshore platform, and they used the lumped mass method to simulate the effect of the TLD on the structure. The results are consistent with the experiment, and they concluded that the TLD could effectively reduce the structure motion during earthquakes. However, the earthquakes were the only loads considered in their study.

In the previous studies, not all the environmental loads, such as wind, waves, and earthquakes, were considered. Therefore, this study proposed setting multiple TLDs on the top of OWTs to reduce the motion of OWTs under various environmental load conditions including wind, waves, and earthquakes. The most recent reported study of Chen and Yang [13] indicated once the natural frequency (ω_l) of a TLD is equal to the exciting frequency (ω_x), the TLD may have the best motion reduction effect. As a result, the natural frequency of the TLD may be tuned to the natural frequency (ω_s) of the OWT, and good motion reduction of the OWT can be expected. The study mainly refers to the International Electrotechnical Commission (IEC) and the internationally renowned certification unit DNV (Det Norske Veritas) [14] for the environmental load simulation and analysis. The supported tower, monopile foundation, and wind turbine models refer to the 5 MW WTs designed by Jonkaman et al. [15] and Jonkman and Musial [16]. Wind and wave loads are generated by the FAST program, which was developed by the National Renewable Energy Laboratory (NREL). The FAST program can perform the wind analysis of the wind turbine during operation, startup, parked, shutdown, and standby states. The turbulent wind field simulation was made by the TurbSim program, which was also developed by NREL. The wind and wave conditions refer to the results of the feasibility study of Taipower's second phase offshore wind power project. The wave conditions are the appropriate wave height and period at the water depth of 20 m in the Changbin offshore project wind field in Taiwan, and the corresponding wind speed is at 90 m elevation. The required wind field and wave conditions were determined according to IEC 61400-3 design load (Design load case) regulations [17].

Turbsim simulates the wind field in the frequency domain using single-point power spectral density, spatial correlation function, and Taylor turbulence hypothesis. The FAST uses the blade element momentum theory to calculate the force of the wind acting on the blade. In this study, the hydrodynamic load evaluation of the supporting structure is referred to the above relevant specifications, and it considered the regular wave and the irregular wave models. After obtaining the dynamic characteristics of the wave particles, the hydrodynamic load can be calculated by using the Morison equation.

The TLDs were set at the top of the tower, and the two-way fluid-solid coupling module of ANSYS was used to simulate the interaction between the TLD and the structure. This study also designed simple experiments to verify the accuracy of numerical simulation. Then, this study explored the effect of TLD on offshore wind turbines under various wind and wave conditions. We also used the rainflow-counting method and the Miner's rule to do the fatigue analysis. Section 2 introduces the methods used in this study and they include FAST and Turbsim, as well as ANSYS-Fluent and ANSYS-Mechanical modules. The environmental loads according to IEC 61400-3 were also described in the section. Section 3 reports the simulation results and experimental measurements and numerical results validation. The effects of multiple TLDs on structural motion control were investigated in the section. The fatigue analysis of OWT with TLDs was also reported in this section. The final section lists the concluding remarks found in this study.

2. Methods Used

FAST is a computer-aided engineering (CAE) software developed by NREL, which is mainly used to simulate the dynamic responses of a wind turbine. FAST incorporates aerodynamic models (AeroDyn), hydrodynamic models of offshore structures (HydroDyn), control and motor system

dynamic models (ServoDyn), and structural dynamic model (ElastoDyn and SubDyn). FAST can simultaneously couple air, fluid, motors, and structures in the same time domain.

2.1. Environmental Loads

The environmental conditions included wind, waves, and current. A full field wind speed above mean sea level (MSL) was established based on the field data measured by the Central Weather Bureau, Taiwan. Regarding hydrodynamic loading, the ocean conditions considered in this study include waves, ocean currents, and water levels.

2.1.1. Wind Model

This study selects the wind speed and wind field model of the wind field according to the IEC 61400-3 specification, and then it uses the TurbSim to simulate the wind field. TurbSim is a random, global, turbulent wind field simulator. Simulating the time series of three wind speed vectors on two-dimensional orthogonal grid points, TurbSim generates the wind spectrum frequency by wind speed, turbulence model, wind field model, etc. Then obtains the time history of the wind field by inverse Fourier transform. The data generated by TurbSim can be used by inputting AeroDyn in FAST. Then, it inputs TurbSim's two-dimensional wind field data in AeroDyn, converts it into a three-dimensional wind field by Taylor's frozen turbulence hypothesis, linearly interpolates the wind speed on the node, and converts it into an external force on the node. The force on the blade is theoretically analyzed by blade element momentum theory, and the blade tip loss correction factor is also considered. The FAST simulation procedure is shown in Figure 1.

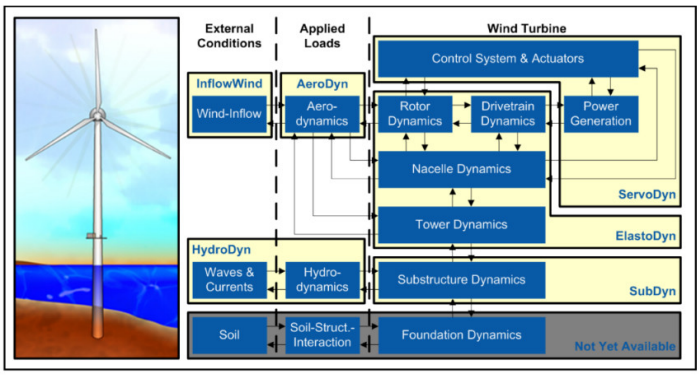

Figure 1. The simulation procedure of FAST (National Renewable Energy Laboratory, or NREL).

The wind load of the rotor nacelle assembly (RNA) and the structure (the tower and substructure are included) were evaluated separately. The wind load of the support structure is based on DNV-RP-C205 (DNV 2014) [18], while FAST analysis provides the wind load of RNA. According to the IEC 61400-1 specification (IEC 2005) [19], the relevant parameters of the standard wind-turbine (WT) class are shown in the Table 1.

Table 1. Wind related parameters of the wind-turbine (WT) classes.

WT class	I	II	III
V_{ref} (m/s)	50	42.5	37.5
Turbulence class	A	B	C
I_{ref}	16%	14%	12%

V_{ref} is the 10-min average wind speed at RNA, and I_{ref} is the turbulence intensity within 10 min.

According to IEC 61400-1, the WT class I-A was adopted, and the reference wind speed V_{ref} and turbulence intensity I_{ref} were set as 50 m/s and 0.16, respectively. The longitudinal turbulence scale parameter Λ_1 is shown in Equation (1) as

$$\Lambda_1 = \begin{cases} 0.7z, & z_{ref} \leq 60\ m \\ 42, & z_{ref} > 60\ m \end{cases} \quad (1)$$

where z is the height above the still water level, and z_{ref} is the height at the RNA center.

The longitudinal standard deviation of the normal turbulence model is the standard deviation of 90% of the average wind speed at the height of the hub (nacelle), and it can be estimated by

$$\sigma_1 = I_{ref}(0.75V_{ref} + b),\ \mathrm{b} = 5.6\ \mathrm{m/s}. \quad (2)$$

The turbulent extreme wind speed model has a 10-min average wind speed of V_{50} and V_1, respectively, in the 50-year and 1-year regression periods:

$$V_{50} = V_{ref}(z/z_{ref})^{0.11} \quad (3)$$

$$V_1 = 0.8V_{50}. \quad (4)$$

The standard deviation of the longitudinal turbulence is:

$$\sigma_1 = 0.11V_{ref}. \quad (5)$$

The annual data for buoys and tidal observations provided by the Central Weather Bureau, Taiwan were used in this paper, and monthly wind speed statistics and hourly wave records were obtained from the Hsinchu Buoy Station and monthly tidal statistics were obtained from the Waipu Tide Station in the Taiwan Strait.

2.1.2. Wave Model

According to the design load case of IEC 61400-3 (IEC 2009) [17], regular waves and irregular waves can be used. Regular waves include linear and nonlinear waves, and the linear wave is applicable when the wave height is small. When the wave height increases or the water depth becomes shallow, the wave peaks become sharp, and the troughs become flat. At this time, the linear wave theory is not enough to describe the waveform and the movement of water particles, so the nonlinear wave should be used, and one can use the streamline function theory to describe nonlinear waves in the most water depths. Once the water depth, period, and wave height were determined, the required wave theory can be determined accordingly (DNV OSJ101, 2014) [18]. Irregular waves usually describe in terms of their spectra, and the JONSWAP and Pierson–Moskowitz spectra are the most commonly used spectra. In this study, the water depth of 20 m was assumed, the stream wave function was used in the regular wave model, and the JONSWAP spectrum was applied to the stochastic irregular wave model.

2.1.3. Current Model

Ocean currents always vary in space and time, but they are usually defined as a uniform horizontal flow field with a direction and flow rate that varies only with water depth. According to IEC 61400-3, the current model is divided into three types: sub-surface currents, near surface currents, and surf underflow currents. In this study, the sub-surface current model was used and they can be expressed as:

$$U_{ss}(z) = U_{ss}(0)\left(\frac{z+d}{d}\right)^{1/7}. \quad (6)$$

The free surface current speed U_{ss} (0) was measured at the OWT site. After selecting the wave theory and current model, the speed and acceleration of water particles can be obtained, and Morison's equation was used to calculate the forces acting on the structure by the waves and currents.

2.2. ANSYS Fluent

ANSYS Fluent is a CFD (Computational Fluid Dynamics) software developed by ANSYS. To study TLDs on the motion reduction for OWT, we combined the fluent and structural analysis modules of ANSYS to simulate the fluid–structure interaction between TLDs and OWTs. We adopted Reynolds-Average Navier–Stokes Equation Models (RANS) and a standard k-ε model to solve the flow passing marine turbines. The detailed description of the model is as follows:

The RANS momentum equations can be written as

$$\rho\left(\frac{\partial \overline{u}_i}{\partial t} + U_k\frac{\partial \overline{u}_i}{\partial x_k}\right) = -\frac{\partial p}{\partial x_i} + \frac{\partial}{\partial x_j}\left(\mu\frac{\partial \overline{u}_i}{\partial x_j}\right) + \frac{\partial R_{ij}}{\partial x_j} \tag{7}$$

where ρ is fluid density, μ is dynamic viscosity, p is pressure, u_i is velocity component, x_i is coordinate, t is time, and R_{ij} is the Reynolds stress. The eddy viscosity model was used, and the Reynold shear stress can be written as

$$R_{ij} = -\rho\overline{u'_i u'_j} = \mu_t\left(\frac{\partial \overline{u}_i}{\partial x_j} + \frac{\partial \overline{u}_j}{\partial x_i}\right) - \frac{2}{3}\mu_t\frac{\partial \overline{u}_k}{\partial x_k}\delta_{ij} - \frac{2}{3}\rho k\delta_{ij} \tag{8}$$

$\delta_{ij} = 1$ when $i = j$ and 0 when $i \neq j$. Lai et al. (2016) used three turbulence models to investigate the optimal turbine blades, and they are the "Realizable k-ε two layer", "standard k-ε", and "k-ε SST". They found that the results of three different models are about the same. Then, we chose the "standard k-ε" model. Then, we have $\mu_t = f(\rho k^2/\varepsilon)$, where k and ε are the turbulent kinetic energy and turbulent kinetic energy dissipation rate, and they can be defined as

$$k \equiv \overline{u'_i u'_j}/2 \text{ and } \varepsilon \equiv \nu\overline{\partial u'_i/\partial x_j(\partial u'_i/\partial x_j + \partial u'_j/\partial x_x)}. \tag{9}$$

Turbulent energy equation of the standard k-ε model equations:

$$\frac{D(\rho\varepsilon)}{Dt} = \frac{\partial}{\partial x_j}\left[\left(\mu + \frac{\mu_t}{\sigma_\varepsilon}\right)\frac{\partial \varepsilon}{\partial x_j}\right] + C_{\varepsilon 1}\frac{\varepsilon}{k}G_k - \rho C_{\varepsilon 2}\frac{\varepsilon^2}{k} \tag{10}$$

where G_k can be defined as

$$G_k = \rho\nu_t\frac{\partial \overline{u}_i}{\partial x_j}\left(\frac{\partial \overline{u}_i}{\partial x_j} + \frac{\partial \overline{u}_j}{\partial x_i}\right). \tag{11}$$

The values of all the constants are empirically as $C_\mu = 0.09$, $C_{\varepsilon 1} = 1.44$, $C_{\varepsilon 2} = 1.92$, and $\sigma_k = 1.0$.

ANSYS Mechanical

ANSYS Mechanical is a CAE (Computer Aided Engineering) software that simulates structural responses by the finite element method. The simulation analysis includes structural strength, stress, vibration, etc., and it can be combined with other ANSYS software for coupling analysis. In some cases, the fluid flow will cause the displacement of the solid, and the displaced solid will change the flow field of the fluid. Fluid–structure coupling is divided into one-way (1-way) and two-way (2-way) fluid–solid coupling. One-way fluid–solid coupling is to treat an already calculated result as another boundary condition to be calculated. Bidirectional coupling is divided into fully coupled, implicit, and explicit coupling. Full coupling calculates the simultaneous equations of fluid and solid as a matrix, which is often difficult to be solved. Implicit coupling is generally used by iteration until the convergence target is reached. Explicit coupling requires very a small time step and is very time consuming; therefore, it is

not recommended. Figure 2 shows the FSI (Fluid-Structure interaction) module of ANSYS, and the implicit method was chosen in this study to perform the fluid–structure coupling analysis.

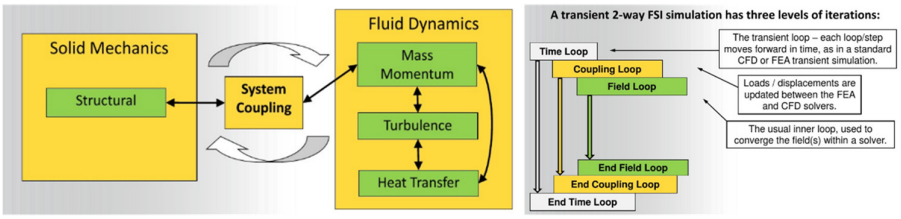

Figure 2. The system coupling and the two-way FSI simulation in ANSYS workbench.

2.3. Monopile OWT

This paper refers to the 5 MW offshore wind turbine developed by NREL. The radius of the three blades is 61.5 m, and the hub height is 90 m above the water surface. The water depth is assumed to be 20 m. The top of the tower has a diameter of 3.87 m and a thickness of 0.019 m. The bottom diameter is 6 m, and the thickness is 0.027 m. The total length of the tower is 77.6 m. The diameter and the thickness of the pile foundation are 6 m and 0.060 m respectively, and the length of the pile foundation is 30 m. The material of the supporting structures is steel, and the properties are as follows: the Young's modulus is 210 GPa, the shear modulus is 80.8 GPa, and the density is 7850 kg/m^3. In this study, the rotor, wind turbine blade, and nacelle are assembled as a lump mass (RNA). Figure 3 shows the 5 MW OWT and the simplified OWT model for the simulation.

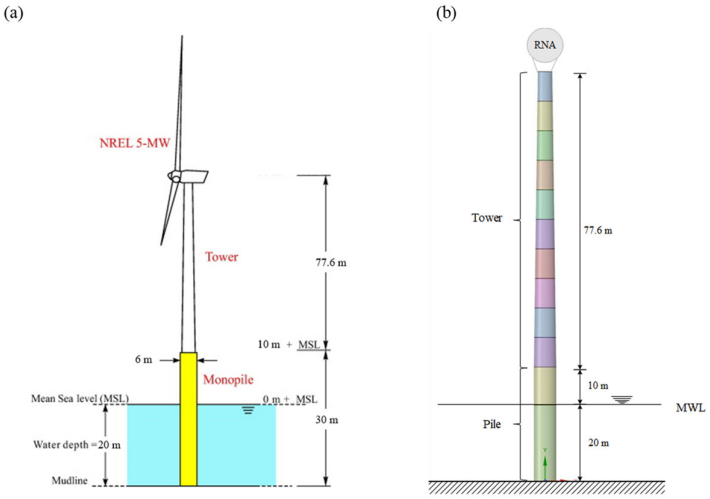

Figure 3. (**a**) The 5 MW offshore wind turbine (OWT) developed by NREL; (**b**) a simplified OWT model.

To reduce the dynamic response of the OWT, a TLD is installed at the top of the OWT. Figure 4 shows the simulation chart. To perform the simulation, the environmental loads were determined first. Since the turbulent wind field was considered, the TurbSim was used to generate a turbulent wind field, and then we input the obtained data to FAST. Then, the force data generated by FAST was input into ANSYS Transient Structural. The TLD geometry was determined based on the tuned frequency of TLD. We used ANSYS Fluent to simulate the sloshing flow in TLD, and then we used system coupling to complete the fluid–structure coupling simulation.

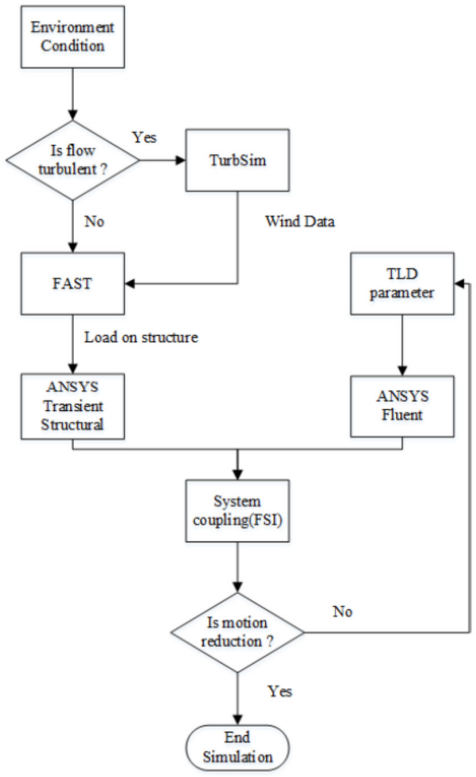

Figure 4. The flow chart of the simuation performed in this study.

One TLD was assumed first, and the simulated responses were compared to those without TLD, and the motion reduction ratio was calculated to evaluate the motion control effect. Different load conditions were assumed, such as harmonic ground motion, real earthquake excitation, coupled wind and wave loads, etc. Once the motion reduction was insignificant, more TLDs (2-TLD and 3-TLD) were then added to evaluate the possible increasing on motion reduction control. For fluid–solid interaction simulation, the SpaceClaim model was imported into Fluent, and the area of the structure was deactivated except for the TLD part. After the meshing was generated, the fluid–solid coupling interface was defined. The VOF calculation and the multi-phase flow were used in Fluent analysis. The turbulence mode was a standard k $-$ ϵ model.

3. Results and Discussion

3.1. Model Validation

Before presenting the numerical simulations made in this study, the experimental measurements were performed to validate the simulation results obtained in this study. A simple experimental model (shown in Figure 5) was set up. The supported tower was a 3-meter height PVC pipe with a diameter of 12 cm. The RNA (rotor nacelle assemble) was replaced by a lump weight of 1 kg. The cylindrical TLD was set at the top of the RNA. The density, Young's modulus, and Poisson's ratio of the PVC pipe are, respectively, 1532 kg/m^3, 3070 MPa, and 0.4. As illustrated in Figure 6, the OWT model was set on a shaking table that can be moved back and forth with an AC motor. The maximum moving distance (r) of the shaking table is ±30 mm, and the highest revolutions of the motor is 2000 r.p.m. The AC motor can reciprocate according to the programmed displacement path and frequency. The motion trajectory of the instrument is based on the sine wave. With a maximum amplitude of ±5 mm reciprocating movement, a circular platform is attached to the square platform on which the OWT was installed. A Keyence laser displacement meter is set at the proper elevation to measure the time history of displacement of the RNA.

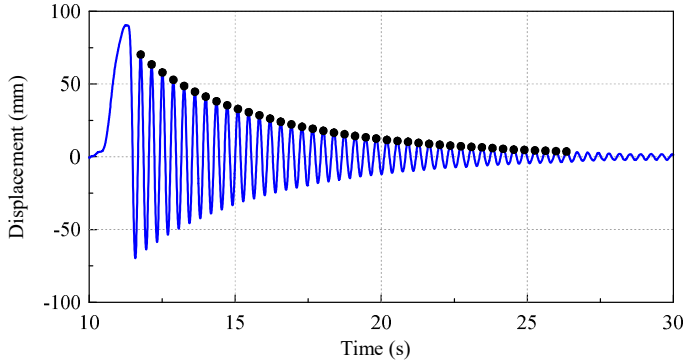

Figure 5. The dynamic displacement decay history of free vibration of a scaled model OWT.

The free vibration experiment was firstly made to evaluate the damping coefficient of the system. Figure 5 shows the decay history of the dynamic displacement, and the damping ratio of the experimental set up can be calculated according to the following equation

$$\ln\left(\frac{x_1}{x_j}\right) = \frac{2\pi j\zeta}{\sqrt{1-\zeta^2}}. \tag{12}$$

According to the decay history, the damping ratio $\zeta = 0.0119$ was determined.

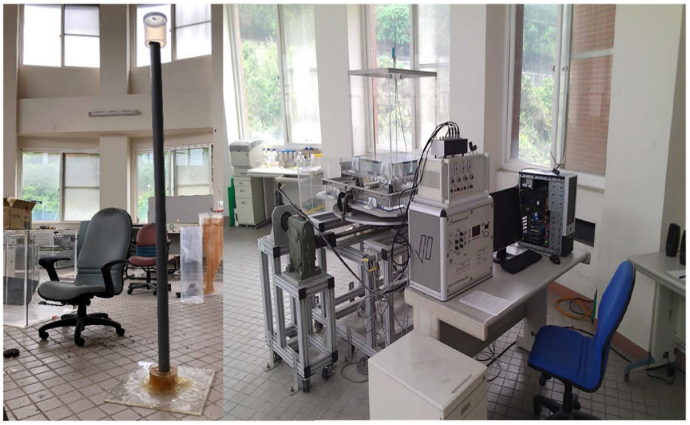

Figure 6. The simple experimental set up of OWT with a tuned liquid damper (TLD) on top.

3.1.1. Simulated Natural Frequency and Dynamic Response Validation

To confirm the accuracy of experimental measurements, the fundamental frequency of the scaled OWT model was checked. The base platform was excited by a harmonic force, $F(t) = A\omega_x \sin(\omega_x t)$, where A is the amplitude of the excitation and ω_x is the excitation frequency. ANSYS was used to calculate the corresponding dynamic displacement response. The ANSYS FEM-Modal set up was based on the experimental model, and the natural frequency of the model was calculated. The calculated natural frequency (2.751 Hz) is very close to the experimental measurement (2.75 Hz). Figure 7 clearly shows the agreement of the simulation and experimental results, and the peak dimensionless displacement occurred when the exciting frequency (ω_x) is equal to the natural frequency (ω_s) of the model, i.e., $\omega_x/\omega_s = 1$. Figure 8 shows the comparison of the dynamic displacement obtained by ANSYS simulation and those of the experimental measurements and the agreement is also very good. The dynamic displacements measured in this section were also used as a reference to evaluate the effects of TLD on the response reduction of the OWT.

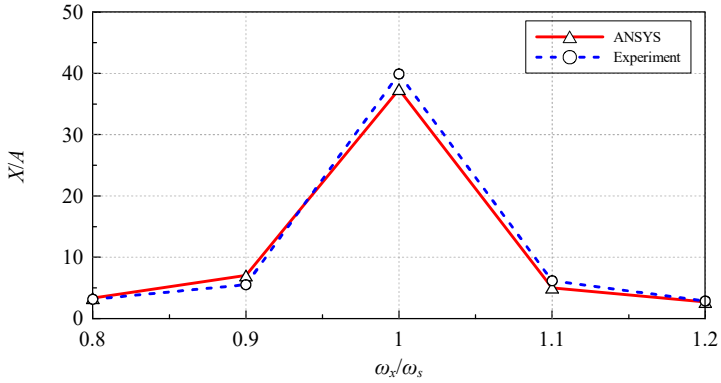

Figure 7. The comparison of ANSYS simulated results and the experimental measurements; X/A: the dimensionless displacement of OWT; $\omega_x/\omega_s = 1$: excitation frequency (ω_x) is equal to the natural frequency of OWT (ω_s).

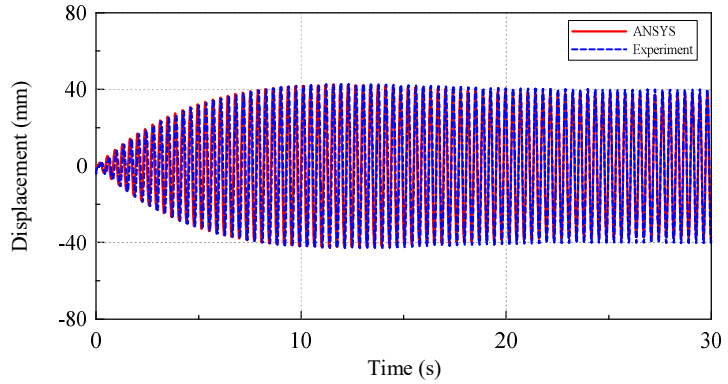

Figure 8. The history of the displacement at the rotor nacelle assembly (RNA) of OWT under excitation wih exciting frequency = natural frequency of the OWT.

3.1.2. Fluent TLD Simulation Validation

In the ANYSY fluid–solid coupling, the accuracy of the hydrodynamic force calculation is important, and Fluent may correctly transmit the force of the fluid acting on the tank wall to the structure. Figure 9 illustrates the comparison of the Fluent-simulated force with the experimental measurements of Krabbenhøft (2011) [20], and the agreement is very good.

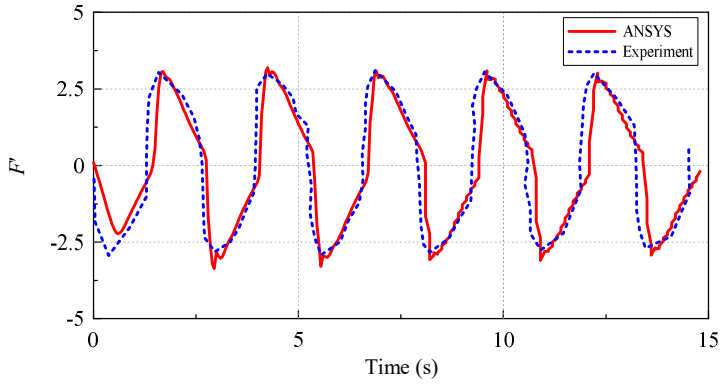

Figure 9. The comparison of the forces acting on the tank wall; solid line: ANSYS results; dashed line: experimental measurements (Krabbenhøft, 2011) [20]. Tank length = 0.59 m, water depth = 0.02 m, the exciting amplitude = 0.02 m, and the exciting frequency = 2.36 rad/s.

3.1.3. ANSYS Mechanical Model (Fluid–Structure Interaction) Validation

The comparison made in the previous sections validated the accuracies of simulations made by the ANSYS Fluent and ANSYS structure models. In this subsection, we further validated the accuracy of the fluent and structure coupling model. The TLD was added on the top of the scaled OWT model, and an experiment was performed to investigate the motion reduction of the OWT.

The exciting force is a harmonic motion, the displacement amplitude is set as 0.001 m, and the exciting frequency is set to equal to the natural frequency of the OWT. ANSYS-Transient-Structural and ANSYS-Fluent are connected to System Coupling for the data transmission setting and time control. Figure 10 illustrates the TLD mesh model and the fluid–structure coupling interface. Figure 11 shows the schematic of the projects included in the simulation of the interaction between the TLD and OWT.

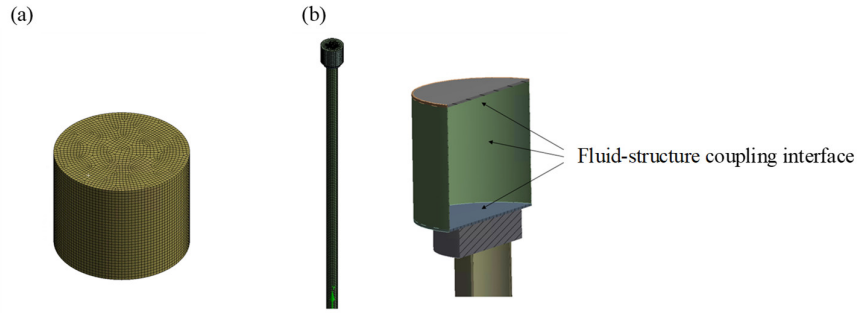

Figure 10. (**a**) The mesh arrangements of fluid in TLD and (**b**) the fluid–structure coupling interface.

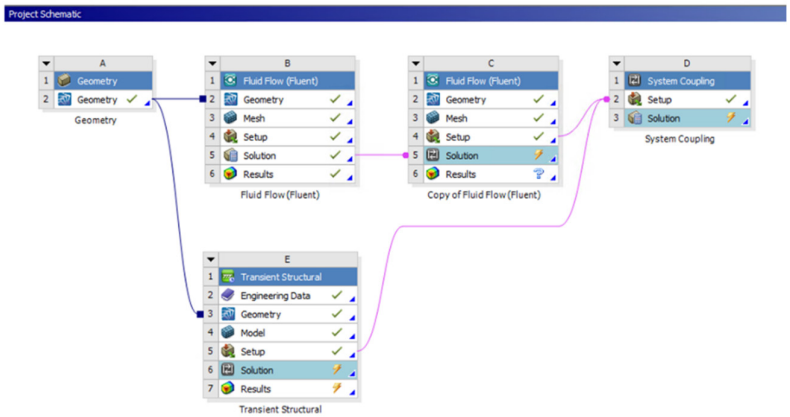

Figure 11. The schematic projects included in the TLD + OWT interaction simulation.

Figure 12 further compares the dynamic displacements of RNA of OWT with and without TLD, and the motion of RNA of OWT is remarkably reduced when the TLD is installed at the top of the RNA of OWT. Figure 13 also shows that the results obtained by ANSYS simulation and the experimental measurements agree very well. The amplitude of the OWT with the TLD is much smaller than that without the TLD; therefore, we use different vertical axes to clarify the difference between the experiment and simulation results. The response of the OWT with the TLD is much more complicated than that without TLD, and more difference between experiment and simulation can be expected, but the deviation is still below 10%. The accuracy of the ANSYS system coupling was confirmed and can be used to study the motion reduction effect of the TLD on the OWT.

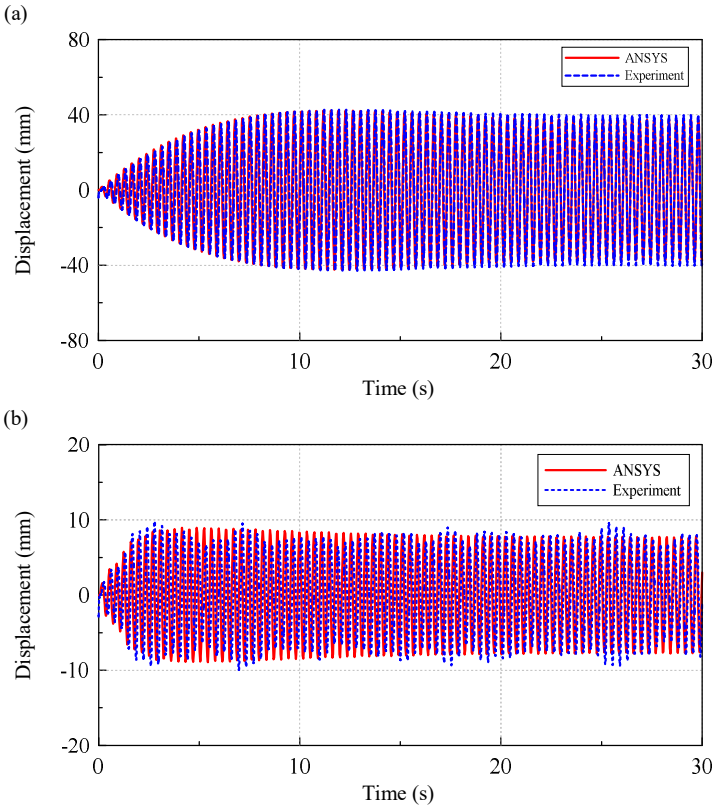

Figure 12. Dynamic displacement of RNA of OWT: (**a**) without TLD; (**b**) with TLD.

3.2. TLD on Motion Reduction of OWT

As shown in Figure 12, the TLD may have a very good motion reduction effect on OWT when it is under a harmonica ground excitation. In the following sections, we will investigate the damping effect of the TLD on the OWT when it is under real environmental load conditions. The design standard IEC 61400-3 defines the load conditions DLC (Design Load Case) for the structural design of offshore wind turbines, including all operating conditions of OWTs, such as startup, normal operation, shutdown, etc. The structural design of the offshore wind turbine often considers the extreme 50-year regression period, while the fatigue analysis is based on the general sea conditions. The environmental loading used in this study refers to the feasibility study of the Taiwan Power Company's offshore wind power generation second phase plan. Table 2 lists the estimated wind and wave conditions and extreme wind and waves at the Zhangbin Industrial Zone project.

Table 2. The wind and wave conditions at the Zhangbin Industrial Zone project. DLC: Design Load Case.

Wind Condition (Elevation 95 m)		Wave Condition (Water Depth 20 m)	
Annual mean wind V_{ave} (m/s) (DLC 1.2)	9.2	H_s (m)	1.4
		T_p (s)	6.1
50 years, V_{ref} (m/s) (DLC 6.2)	54.16	H_{s50} (m)	8.24
		T_{p50} (s)	12.1

3.2.1. Wind Field Simulation

As mentioned in the previous sections, TurbSim was used to simulate the turbulent wind field of the whole domain, and the output binary file was directly used by AeroDyn in FAST. The input parameters of TurnSim are shown in Table 3.

Table 3. Input file description (Turbsim) (DLC 1.2).

Parameter	Description	Value
WrADHH	Output format for AeroDyn	TRUE
NumGrid_Z	Vertical mesh number	31
NumGrid_Y	Horizontal mesh number	31
TimeStep	Time-step (s)	0.05
AnalysisTime	Analysis time (s)	630
UsableTime	Usable time (s)	100
HubHt	Hub height (m)	90
GridHeight	Vertical domain height (m)	145
GridGridWidth	Width of domain (m)	145
TurbModel	Turbulence model	IECKAI
IECstandard	IEC version, IEC-61400-3	3
IEC_WindType	IEC wind type	NTM
RefHt	Reference height (m)	95
URef	Wind-speed at reference height (m/s)	9.2

For the wind field condition of DLC 6.2, the U_{ref} is changed to 54.16 m/s, and the generated file was submitted to AeroDyn to expand into a global wind field. In the AeroDyn, the direction of the wind can be set. In the case of the annual average wind speed of the wind field conditions of the DLC 1.2, the wind turbine directly faces the windward direction, so the wind direction angle is set to 0°. In the extreme load DLC 6.2, the side winds of the 10-year average extreme wind speed and the 50-year regression period are blown toward the blades, so the wind direction angle is set to 90°. Figure 13 shows the wind speed in three directions with an annual average wind speed at 90 m elevation. Since the annual average wind speed is blown toward the wind turbines, the wind speed in the x direction is greater than the other two. Figure 14 shows the corresponding 10-min average extreme wind speed in a 50-year regression period. The wind field is designed to have a crosswind effect on the wind turbines, so the wind speed in the y direction is the largest. The fatigue load in DLC 1.2 is in normal operation, and the turbine blades rotate normally, but in the DLC 6.2 limit load condition, the wind turbine is parked because of excessive wind, and the blade is turned parallel to the wind to reduce the force on the blades. Meanwhile, in the FAST setting, the blades are parked, and the blade angle is set to 90°. Therefore, we may expect that RNA has larger force in the x direction, whereas at extreme wind speeds, RNA has larger force in the y direction, since the wind blows from the y direction.

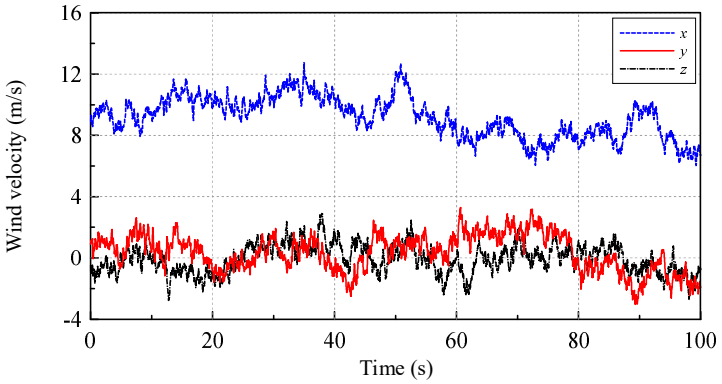

Figure 13. Annual wind speed V_{ave} = 9.2 m/s at 90 m elevation.

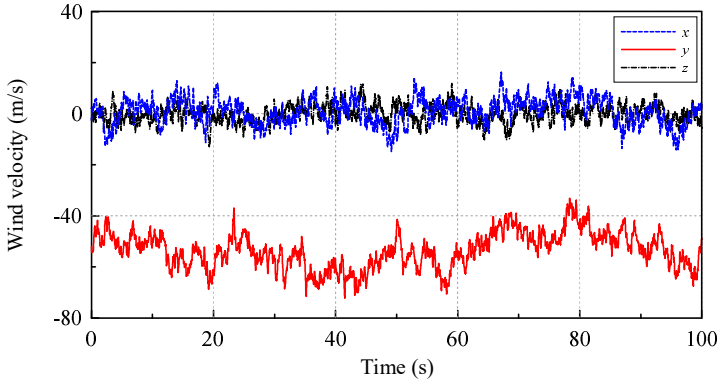

Figure 14. 50-year, 10 min average extreme wind speed V_{ref} = 54.16 (m/s) at 90 m elevation.

3.2.2. Wave Simulation

In FAST, HydroDyn is used to calculate hydrodynamic loads. The regular wave and irregular wave can be selected. In the wave condition of fatigue load, an irregular wave is selected. The PM wave spectrum was selected for the normal sea state, whereas the JONSWAP spectrum is selected for the ultimate load condition, because the JONSWAP spectrum can show the characteristics of extreme sea conditions. Figure 15 shows the wave histories of normal and extreme sea states.

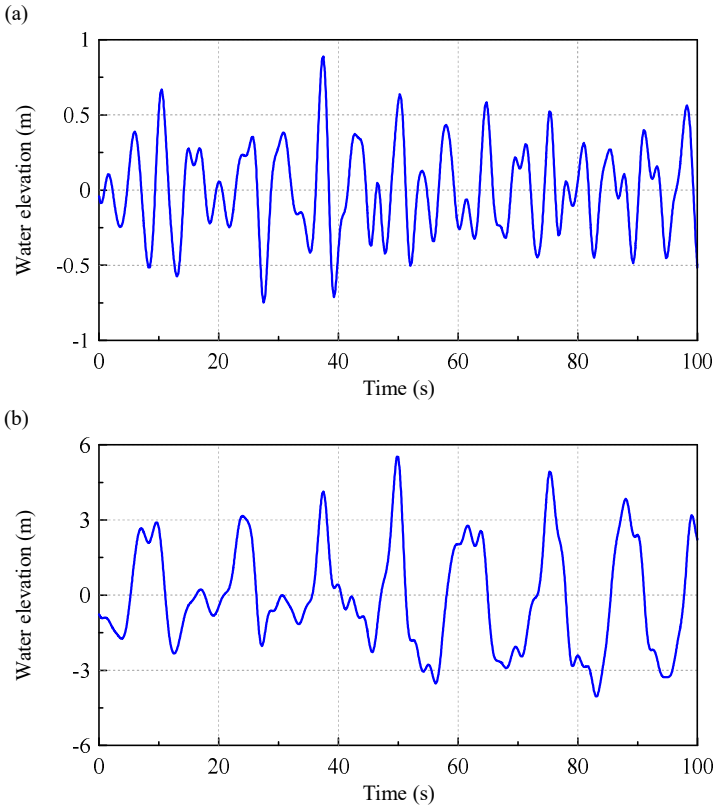

Figure 15. (**a**) Normal wave condition, H_s = 1.4 m, T_p = 6.1 s; (**b**) 50-year extreme wave condition, H_s = 8.24 m, T_p = 12.01 s.

3.2.3. Structural Load

The forces exerted on the OWT can be further calculated by FAST once the wind field and wave fields were established. The OWT includes a rotor, a nacelle, a tower, and a pile. The focus of the study is on the tower, which does not consider the pile part and the deformation of the blade and the

rotational speed of the blades. Therefore, the rotor, the blade, and the nacelle are combined here (RNA) as a lump mass point.

3.2.4. The Loads on RNA

Figure 16 shows the forces of the RAN acting on the top of the tower in DLC 1.2 and DLC 6.2 conditions, respectively. As shown in the figure, RNA has larger force in the x direction for the average wind speed condition, whereas at extreme wind speeds, RNA has larger force in the y direction, since the wind blows from the y direction.

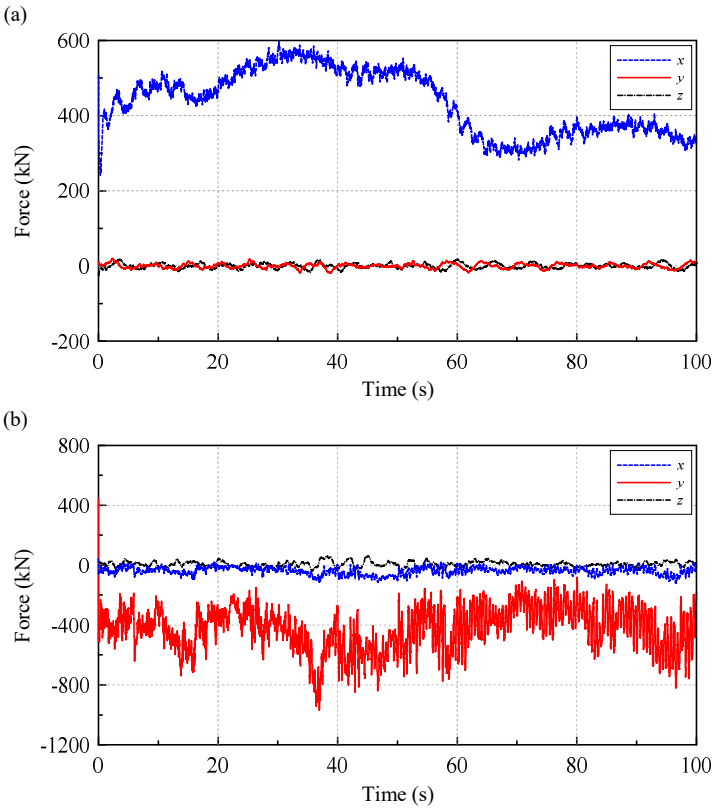

Figure 16. The forces on RNA: (**a**) normal wind condition; (**b**) extreme wind condition.

3.2.5. The Loads on Wind Tower

It can be seen from Figure 6 that the tower with a total length of 77.6 m in FAST is divided into 10 sections, and the length of each section is 7.76 m. The force of the tower is calculated by AeroDyn; Figure 17 depicts the force acting on each tower section at the average wind speed condition, and the force in the x direction is obviously greater than in the other directions. Figure 18 depicts the corresponding forces under extreme wind speed, and the force in the y direction is the largest among all directions.

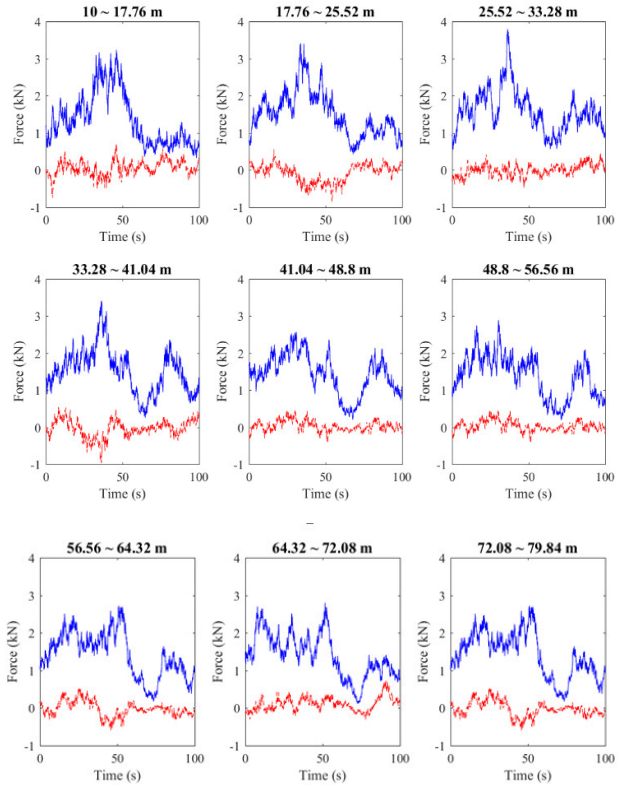

Figure 17. The force on each section of the tower under normal wind conditions (blue line: x direction; red line: y direction).

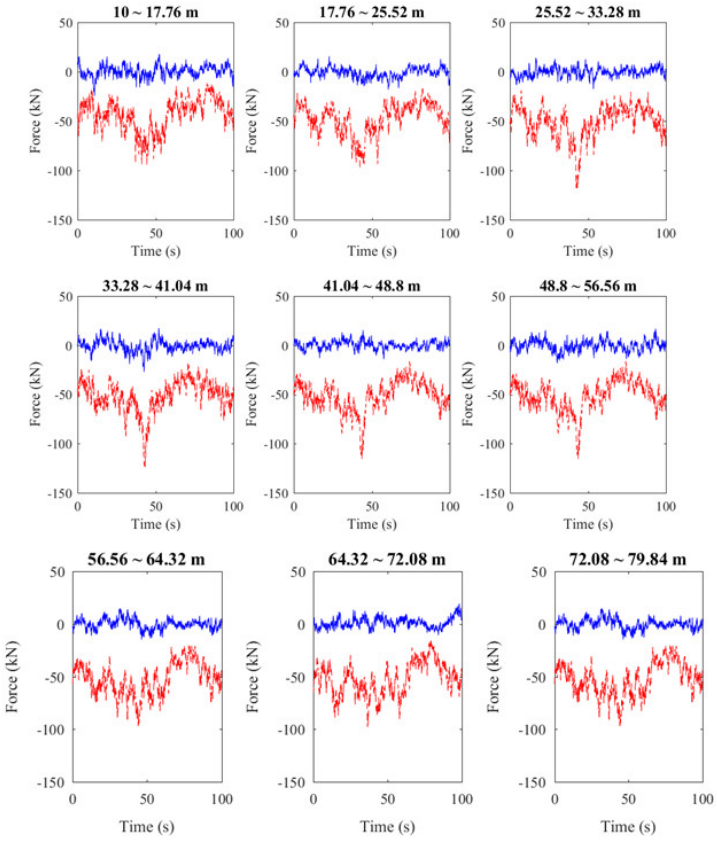

Figure 18. The force of each section of the tower under extreme wind conditions (blue line: x direction; red line: y direction).

3.2.6. The Loads on Pile of the OWT

The length of the supported pile of the OWT is 30 m and it is fixed on the sea bottom, and 20 m and 10 m of it are below and above the sea surface, respectively. HydroDyn is used to calculate the force of the wave on the pile. Figure 19 shows the corresponding forces applied on the pile.

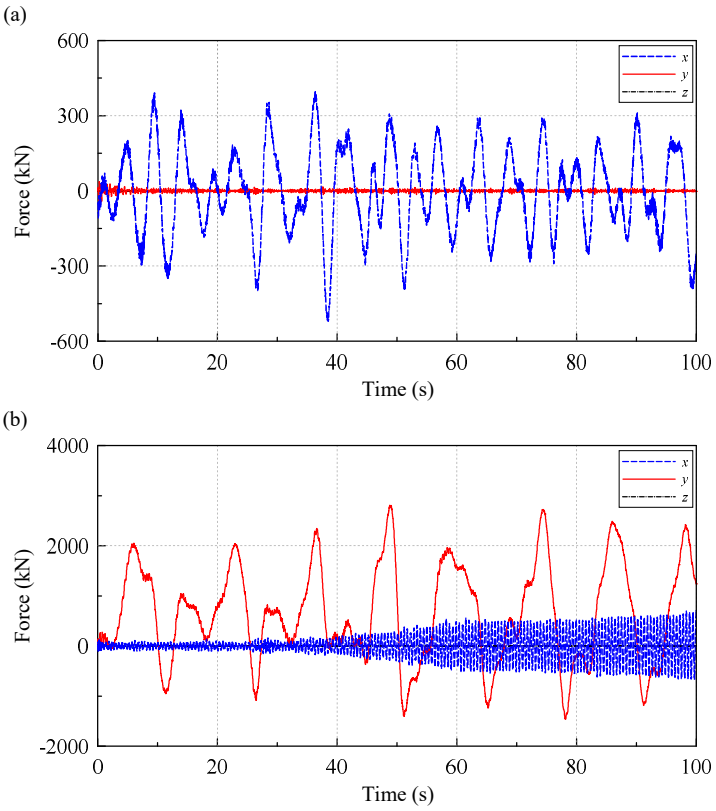

Figure 19. Force applied on the pile of the OWT: (**a**) normal wave condition; (**b**) extreme wave condition.

3.2.7. Tuned Frequency of TLD

As reported in Chen and Hunag (2015) [21] and Chen and Yang (2018) [13], the best motion reduction effect of TLD on the structure may occur when the natural frequency of the TLD is tuned to the frequency of the exciting forces. The effect of waves on the tower top displacement is much less than that of wind, so it is useless to tune the frequency of the TLD to the frequency of waves. In addition, because turbulent wind is a random variable, we did a spectrum analysis of the wind and found that no specific peak exists, so it is not feasible to tune the TLD frequency to the frequency of the wind. However, tuning the frequency of the TLD to the frequency of the structure also has a good damping effect (Chen and Huang, [21]; Frandsen, [22]). Therefore, the natural frequency of the TLD used in this study was tuned to the fundamental frequency of the supported tower of the OWT.

3.2.8. The Displacement of Tower Top

The calculated forces in the previous section were applied to the finite element method (FEM) model of ANSYS. The dynamic response of offshore wind turbines, including the deformations and the stresses of piles and towers, were calculated in this section. Figure 20 shows the displacements of the top of the tower under DLC 1.2 and DLC 6.2 conditions.

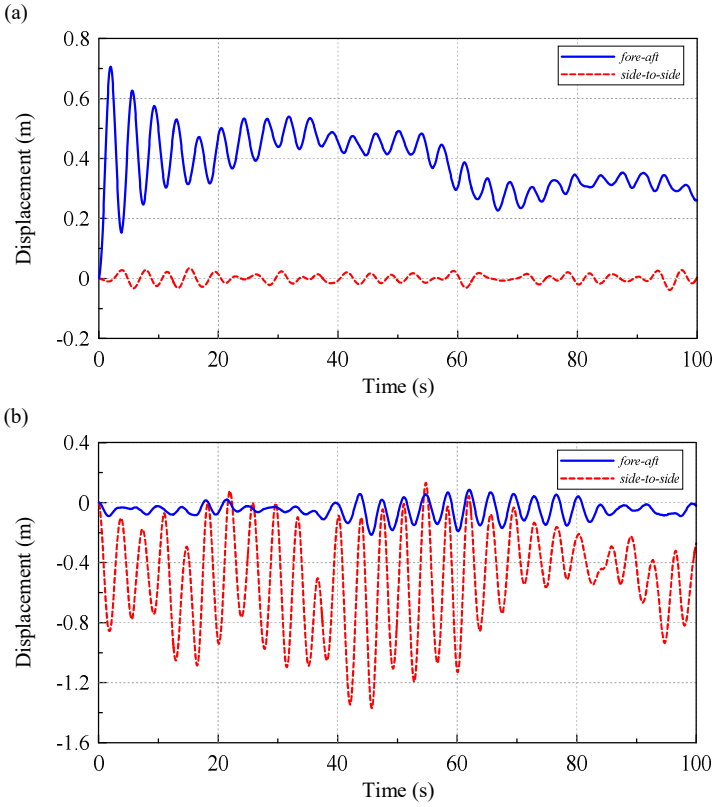

Figure 20. The displacement of the tower top in (**a**): DLC 1.2 condition; (**b**) DLC 6.2 condition.

3.3. TLD Application on Motion Reduction of OWT

The monopile offshore wind turbine is subject to wind and wave loads, which may cause dynamic responses of the structure. This study tried to install the cylindrical TLD on the top of the offshore wind turbine, as shown in Figure 21, to suppress those responses. The diameter of the TLD is 3.846 m, which is about the same size of the inner diameter of the tower top. The natural frequency of the liquid in the cylindrical tank can be calculated by $\omega^2 = \frac{\lambda g}{R}\tanh\frac{\lambda h}{R}$. The water depth of TLD can be determined when we tune the natural frequency of TLD to be equal to the natural frequency of the structure; then, the water depth of TLD = 0.35 m was calculated.

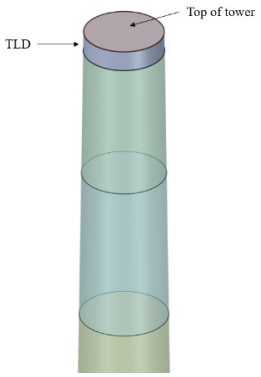

Figure 21. The conceptual sketch of the TLD on the top of the tower.

The mechanical properties of the OWT are shown in Figure 22. The OWT model is drawn by ANSYS SpaceClaim and TLD was also added, which were all input to the Transient Structural. In the Transient Structural, the parameters of the material such as density, Young's modulus, and damping

coefficient, etc. were set. Then, the FAST-calculated wind and wave loads were input. The fluid–solid coupling interface was set as shown in Figure 23.

	A	B	C
1	Property	Value	Unit
2	Material Field Variables	Table	
3	Density	8500	kg m^-3
4	Damping Factor (β)		
5	k-Matrix Damping Multiplier	0.01152	
6	Isotropic Elasticity		
7	Derive from	Young's Modulus and Pois...	
8	Young's Modulus	2.1E+11	Pa
9	Poisson's Ratio	0.3	
10	Bulk Modulus	1.75E+11	Pa
11	Shear Modulus	8.0769E+10	Pa
12	Tensile Yield Strength	3.55E+08	Pa

Figure 22. Transient Structural (the parameters setting).

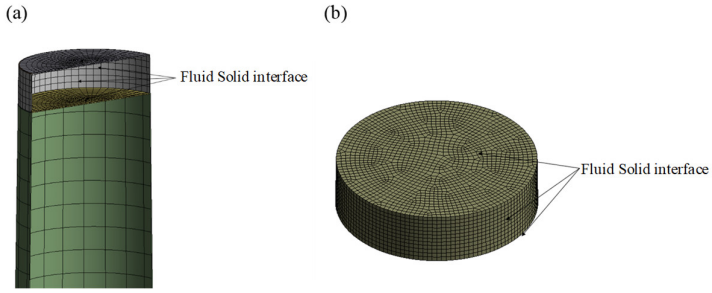

Figure 23. Fluid–solid interface.

Then, the SpaceClaim model was imported into Fluent, and the area of the structure was deactivated except the TLD part. After the meshing was generated, the fluid–solid coupling interface was defined. The VOF calculation was started in Fluent to simulate the multi-phase flow, and the solid boundary was set as the wall. The turbulence mode was a standard k-ε model. In general multi-phase flow, air and water are often set as incompressible fluids to simplify the model, but in the fluid–structure interaction calculation, the boundary of the fluid changes with the solid and the volume of the fluid changes with time, which is very prone to problems in the calculation of Fluent, so it is necessary to set the air as an ideal compressible gas to avoid problems in calculation.

3.3.1. Convergence Test

In order to save calculation time, a hexahedral structural mesh is used here. Three difference mesh sizes (1.4 m, 1.0 m, and 0.7 m) were used to do the convergence tests, and the DLC 6.2 conditions were used as the external force conditions. Table 4 lists the comparison of the root square of displacements of RNA of various mesh sizes used, and all the results were about the same; the mesh size = 1.4 m was selected in the later simulation. Table 5 lists the convergence tests for mesh selection for TLD simulation, and the results of 0.09 m and 0.06 m are about the same and therefore, the mesh size = 0.09 m was selected in the later simulation. The time steps = 0.005 s and 0.0025 s were tested, and the results are about the same, and the time step = 0.005 s was used in the later simulations.

Table 4. The convergence test for tower FEM mesh selection.

Mesh Size (m)	Mesh Number	Root Square of Displacement (m)	Relative Difference with 0.7 m (%)
1.4	3956	0.86877	0.1
1.0	7502	0.86827	0.05
0.7	14,950	0.86784	0

Table 5. The convergence test for TLD mesh selection.

Mesh Size (m)	Mesh Number	Root Square of Displacement (m)	Relative Difference with 0.06 m (%)
0.3	940	0.63282	2
0.09	19,572	0.62020	0.035
0.06	61,778	0.62041	0

3.3.2. TLD on Motion Reduction of OWTs

As shown in Figure 14, the TLD has a significant motion reduction effect when OWT is under a harmonic excitation. While the OWTs are mostly under wind and wave loads, in this section, we investigated the motion reduction effects of TLD on OWT when it is under DLC 1.2 and DLC 6.2 load conditions. Figure 24 illustrates the time histories of fore-aft and side-to-side displacement of RNA of OWT with and without TLD. Although the results presented in the Figure 25 do not show obvious damping effects of TLD on OWT motion reduction, Figure 26 shows the FFT of the displacement responses and indicates that the TLD may reduce response peak intensity by 44% and 24% in fore-aft and side-to-side displacements, respectively. When the environmental load condition DLC 6.2 was applied, the results shown in Figure 27 clearly demonstrate the effects of TLD on the motion reduction of OWTs.

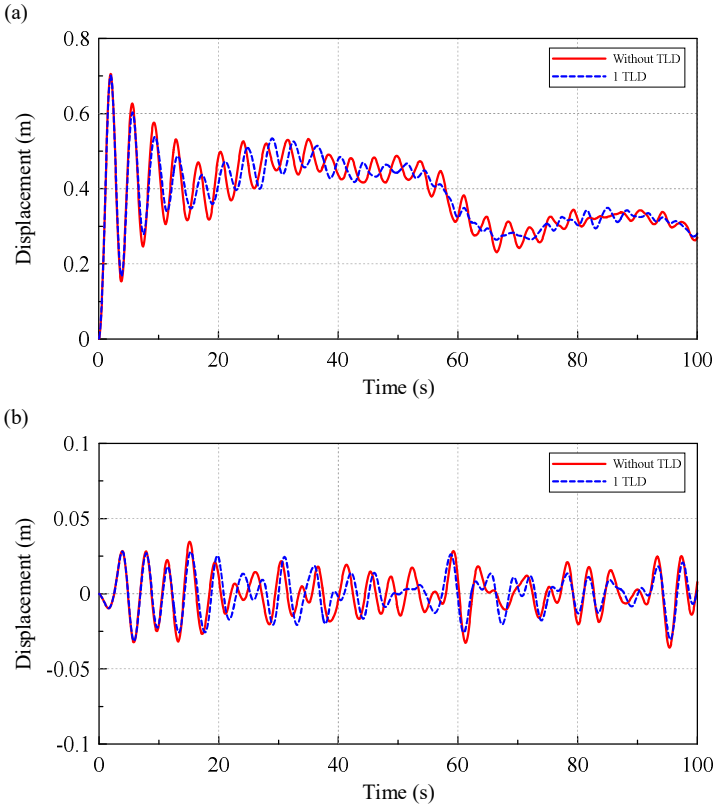

Figure 24. Displacement of RNA for an OWT under the DLC 1.2 condition: (**a**) fore-aft movement; (**b**) side-to-side movement.

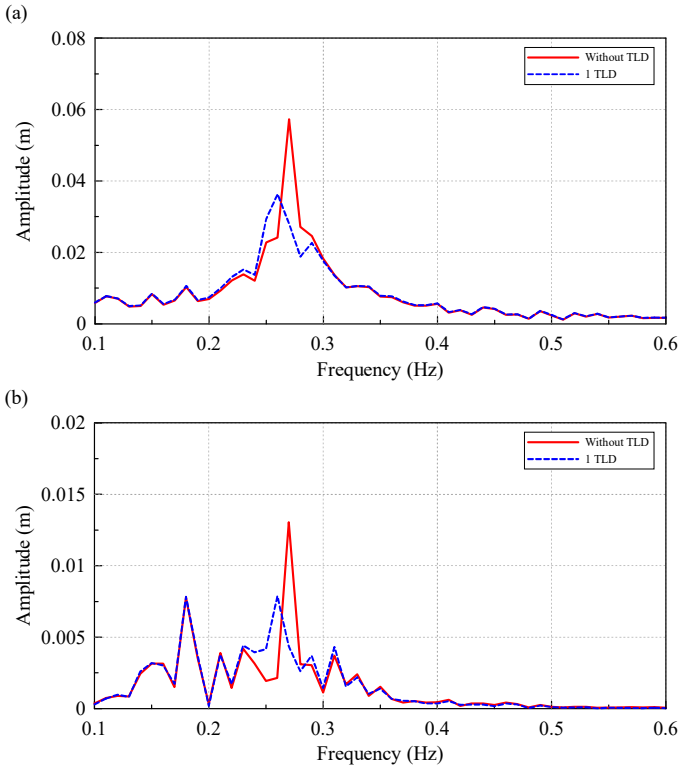

Figure 25. Amplitude spectrum of RNA displacement for an OWT under the DLC 1.2 condition: (**a**) fore-aft movement; (**b**) side-to-side movement.

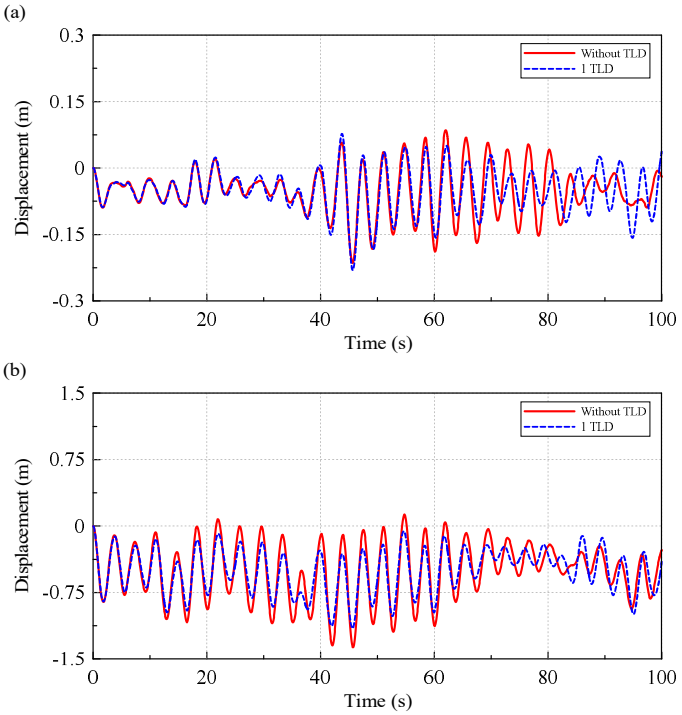

Figure 26. Displacement of RNA for an OWT under the DLC 6.2 condition: (**a**) fore-aft movement; (**b**) side-to-side movement.

3.3.3. Multiple TLDs on Motion Reduction of OWTs

In the previous section, one TLD presents mild motion reduction effects on OWT when it is under DLC 1.2 and DLC 6.2 load conditions. As reported in Chen and Yang's study, the best damping effect of

TLD on the structure might occur when the natural frequency of TLD is tuned to the natural frequency of the structure. Since the OWT is a slender structure and the natural frequency is small, therefore, the water depth of the liquid in TLD is also small. The damping effect of a single TLD might be limited. Then, we increase the number of TLDs, which all have same natural frequency as the natural frequency of the structure. Figure 27 shows the motion reduction effect of multiple TLDs on OWTs when it is under harmonic ground excitation, and the 3-TLD has the best motion reduction effect, which is nearly 100% better than that of the 1-TLD.

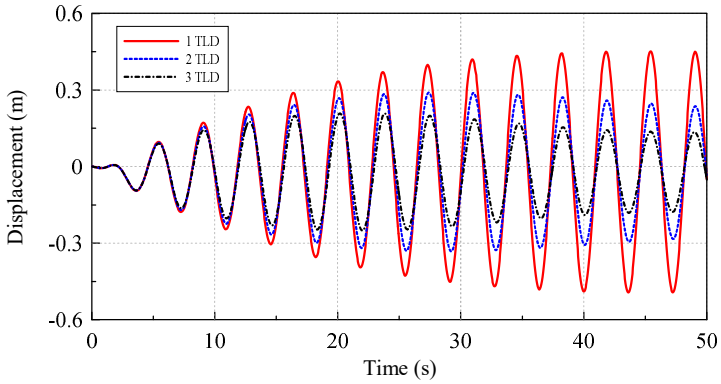

Figure 27. Multiple TLDs on OWT motion reduction and harmonic ground excitation.

As mentioned by Jin et al. (2007) and the results obtained in this study, the TLD did have an excellent motion reduction effect on OWT when it is under harmonic ground excitation. Meanwhile, the environmental loads that OWT may experience include wind, waves, and real earthquakes. Then, we further investigated the motion reduction effects of the multiple TLDs on OWT when it is under real earthquake, wind, and wave loads. Figure 28 depicts the comparison of the damping effects of various TLDs on an OWT under DLC 1.2 and DLC 6.2 load conditions. The motion reduction effects of various TLDs are about the same when the OWT is under DLC 1.2 load conditions. Figure 28 even shows larger peak performance for the 3-TLD, whereas the narrower band can be found for the 3-TLD, and the root mean square of the FFT spectrum of three cases (1-TLD, 2-TLD, and 3-TLD) are about the same in the DLC1.2 condition. The response of OWT under DLC 1.2 is virtually small, and the difference among various TLDs is also insignificant. The force of the DLC 6.2 condition is much larger in the y-direction, and thus, the side-to-side displacements were shown in Figure 28 when the OWT was under the DLC 6.2 condition. The much larger displacement occurred when the OWT was under extreme loading condition (DLC 6.2), and the effect of TLD on motion reduction control became more obvious; more TLDs also enhance the reduction effects. The corresponding comparison of OWT under real earthquakes is shown in Figure 29, and 3-TLD also has the best motion reduction effects among others.

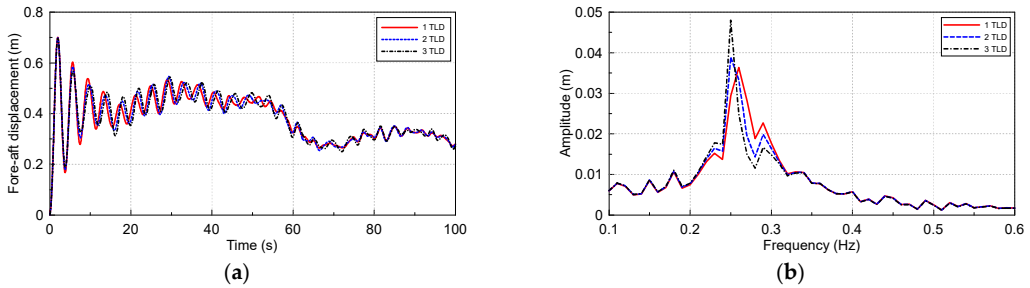

Figure 28. *Cont.*

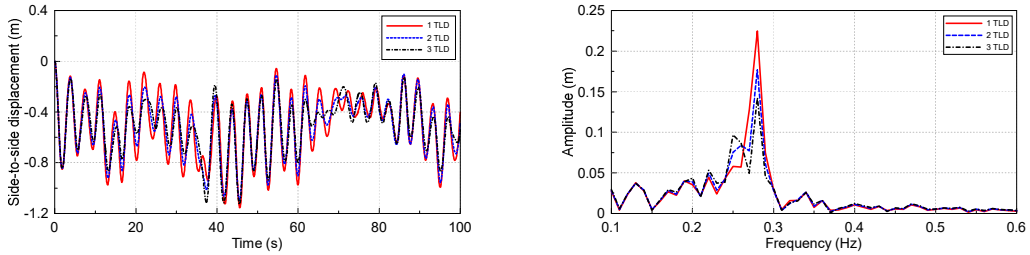

Figure 28. (**a**) and (**b**): The fore-aft displacement and corresponding amplitude spectrum of OWT with various TLDs under the DLC 1.2 condition; (**c**) and (**d**): The side-by-side displacement and corresponding amplitude spectrum of OWT with various TLDs under the DLC 6.2 condition.

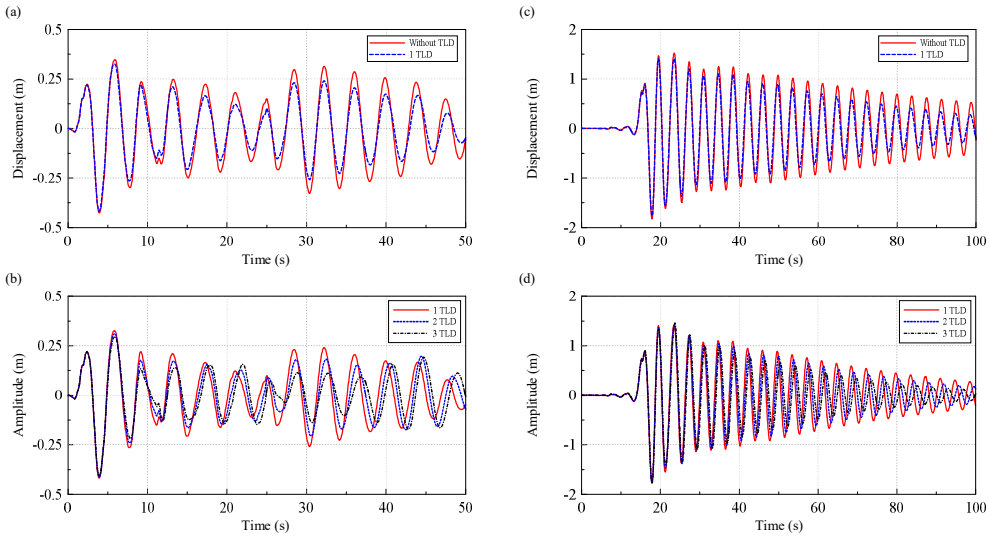

Figure 29. The side-to-side displacement of the OWT with various TLDs: (**a**) and (**b**), El-Centro earthquake; (**c**) and (**d**), Chi-chi earthquake.

3.4. Fatigue Analysis

Figure 30 shows the location where the maximum stress occurs in the absence of TLD according to ANSYS simulation. This position is the intersection of the tower and the pile. Then, we made the fatigue analysis of the stress at the junction of the tower and the supported pile. Figure 31 shows the time series of the maximum stress at the intersection of the tower and the pile.

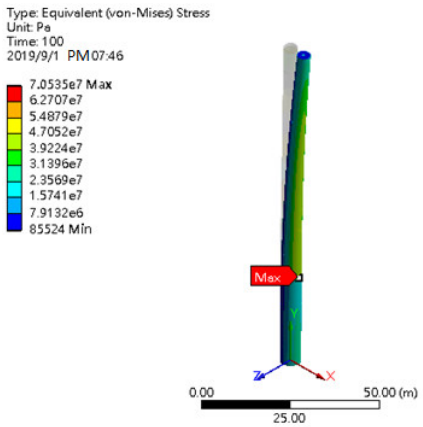

Figure 30. The location of the maximum stress occurred in the OWT.

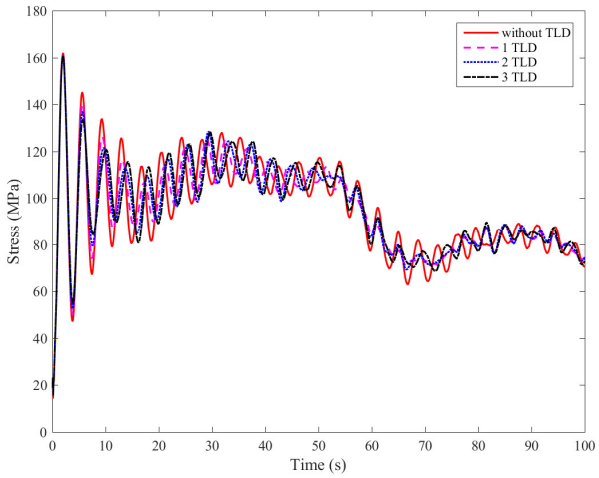

Figure 31. The comparison of the history of the stress at the interaction of the tower and pile of the OWT with various numbers of TLDs.

For a typical offshore structure, the fatigue load history spans a period of 20 years corresponding to about 10^8 wave load cycles (an average wave load period of 6 s). We used the S-N curve to determine the fatigue life at the interaction of tower and pile of the OWT (Ju et al. [23]). In this study, the S-N curve (structural detail class E) of DNVGL-RP-C203 [18] was used to assess the fatigue damage at the interaction of the tower and pile of the OWT. The S-N curve can be expressed as follows

$$\log N = \log \bar{a} - m \log \Delta\sigma \tag{13}$$

where N = predicted number of cycles to failure for stress range; m = the negative inverse slope of the S-N curve; and $\log \bar{a}$ = the intercept of log N-axis by the S-N curve. Table 6 lists the details of the parameters of the S-N curve.

Table 6. S-N curves for tower and pile (Structural detail class E).

Environment	m_1	$\log \bar{a}_1$	m_2	$\log \bar{a}_2$
Air	$N \leq 10^6$ cycles		$N \geq 10^6$ cycles	
	3.0	11.61	5.0	15.35

The rainfall counting was used to obtain the stress counting. The Miner cumulative damage theory was used to estimate the degree of damage to the structure. The Miner's rule states that if there are k different stress levels (with linear damage hypothesis) and the average number of cycles to failure at the ith stress, S_i, is N_i, then the damage fraction, C can be expressed as

$$\sum_{i}^{k} \frac{n_i}{N_i} = C \tag{14}$$

where n_i is the number of cycles accumulated at stress S_i and C is the fraction of life consumed by exposure to the cycles at the different stress levels. Usually, fatigue damage occurs when $C > 1$.

Figure 32 shows the histogram of stress rainflow counting of the uncontrolled OWT and controlled OWT with difference numbers of TLDs. Finally, we apply the Miner cumulative damage theory and S-N curve to infer the fatigue damage value of the OWT. Table 7 lists the fatigue life evaluated based on Miner's rule of uncontrolled OWT and OWT with different numbers of TLDs, and an OWT with 3 TLDs may increase the fatigue life for 20 years. The OWT with a single TLD can also increase the

fatigue life for 13 years. The 3-TLD can not only reduce the motion response but also increase the fatigue life (37% more) of the OWT.

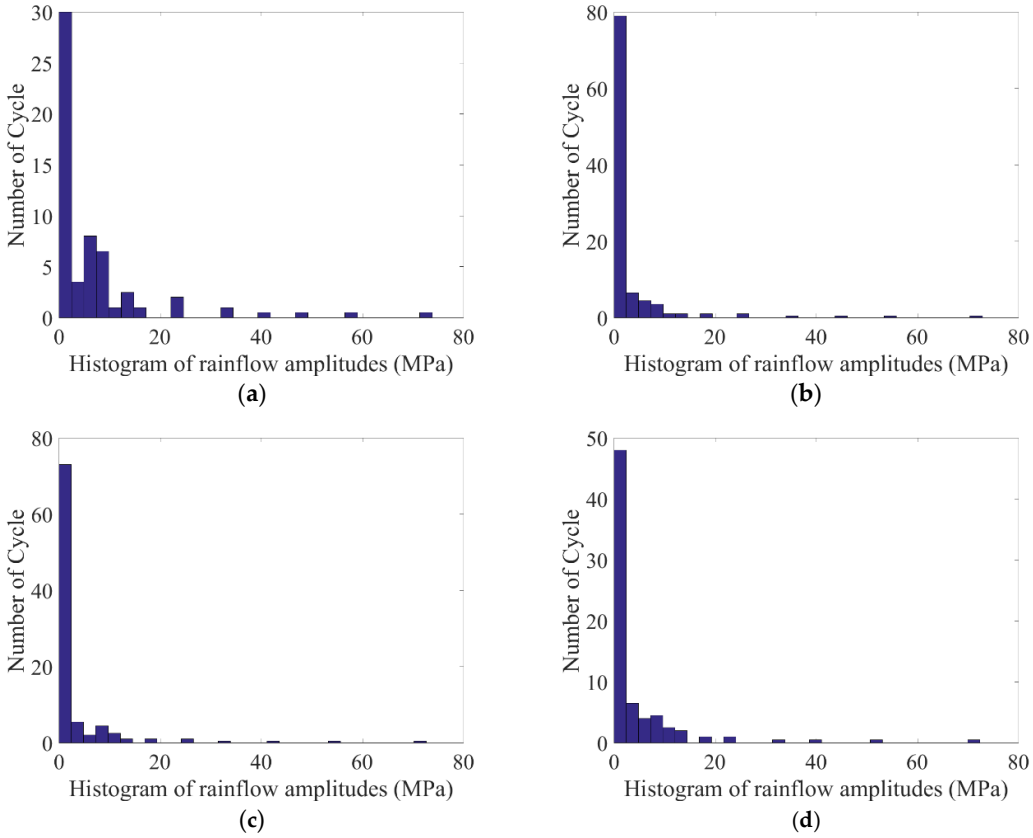

Figure 32. The histogram of stress rainflow counting of uncontrolled OWT and controlled OWT with difference numbers of TLDs.

Table 7. Fatigue life of using various TLDs.

Number of TLD	Fatigue (year)
NO TLD	54.03
1-TLD	67.21
2-TLD	71.25
3-TLD	74.47

4. Conclusions

This study used NREL developed FAST and Turbsim software to generate the environmental loads, which were based on the regulation code IEC 61400-1 and 3. ANSYS-Fluent and ANSYS-Mechanical modules were also used to perform the fluid–structure interaction between OWT and TLDs. The convergence tests and numerical simulation validation were made to confirm the accuracy of the simulation tools used in the study. Extensive simulation cases were made, and the following conclusion were found.

(1). A sample simulation was made to valid the readiness of using FAST, and a simple experimental model was set to perform the numerical validation of accuracy of the ANSYS simulation.

(2). The experimental measurements confirm the significant structural motion control effects of TLD on OWT under a harmonic ground excitation.

(3). The motion reduction effect of a single TLD was studied first. The FFT of the displacement responses of OWT under DLC 1.2 loads indicates that the TLD may reduce response peak intensity

by 44% and 24% in fore-aft and side-to-side displacements, respectively. Similar damping effects of TLD can be found in DLC 6.2 load conditions.

(4). The simulation of the multiple TLDs setting was also made. When the OWT is under harmonic ground acceleration, the natural frequency is easily tuned to equal to the ground exciting frequency, and the simulation results show that better motion reduction control (almost 100% better) can be achieved when the number of the TLD is increased from 1 to 3. Meanwhile, for real earthquake excitation, the frequency contents are various, and the motion reduction effects of multiple TLDs on an OWT under real earthquake conditions are not as significant as those of an OWT under a harmonic excitation.

(5). The motion reduction effects of various TLDs are about the same when an OWT is under DLC 1.2 load conditions, whereas the reduction effect of a 3-TLD is the best among others when the OWT is under DLC 6.2 loading conditions. The corresponding comparison of an OWT under real earthquakes also indicates that 3-TLD has the best motion reduction effects.

(6). The fatigue analysis shows that the fatigue life of an OWT may increase 37% when a 3-TLD was installed. The multiple TLDs are recommended and may be applied on the structural motion control of OWTs.

(7). As a result of the time-consuming nature of the calculation, the environmental conditions of this study only picked DLC 1.2 and DLC 6.2 for simulations. In IEC 61400-3, there are many different DLCs, of which DLC 6.2 also has many different wind and wave angles. More simulations can be made, and the effectiveness of the proposed direction-free TLD application may be further confirmed.

Author Contributions: Conceptualization, B.-F.C.; methodology, B.-F.C. and S.-H.C.; software, S.-H.C.; validation, S.-H.C. and P.-H.Y.; writing—original draft preparation, S.-H.C. and B.-F.C.; writing—review and editing, B.-F.C. and P.-H.Y.; visualization, P.-H.Y.; supervision, B.-F.C. and P.-H.Y.; project administration, B.-F.C.; funding acquisition, B.-F.C. All authors have read and agreed to the published version of the manuscript.

Funding: This study is partially supported by a grant of Ministry of Science and Technology of ROC under a grant-number MOST-102-2221-E-110-039-MY3.

Conflicts of Interest: The authors declare no conflict of interest.

References

1. Murtagh, P.J.; Ghosh, A.; Basu, B.; Broderick, B.M. Passive control of wind turbine vibrations including blade/tower interaction and rotationally sampled turbulence. *Wind Energy Int. J. Prog. Appl. Wind Power Convers. Technol.* **2008**, *11*, 305–317. [CrossRef]
2. Sun, C.; Jahangiri, V. Bi-directional vibration control of offshore wind turbines using a 3D pendulum tuned mass damper. *Mech. Syst. Signal Process.* **2018**, *105*, 338–360. [CrossRef]
3. Hemmati, A.; Oterkus, E. Semi-active structural control of offshore wind turbines considering damage development. *J. Mar. Sci. Eng.* **2018**, *6*, 102. [CrossRef]
4. Modi, V.J.; Welt, F. Damping of wind induced oscillations through liquid sloshing. *J. Wind Eng. Ind. Aerodyn.* **1988**, *30*, 85–94. [CrossRef]
5. Fujii, K.; Tamura, Y.; Sato, T.; Wakahara, T. Wind-induced vibration of tower and practical applications of tuned sloshing damper. *J. Wind Eng. Ind. Aerodyn.* **1990**, *33*, 263–272. [CrossRef]
6. Kareem, A. Reduction of wind induced motion utilizing a tuned sloshing damper. *J. Wind Eng. Ind. Aerodyn.* **1990**, *36*, 725–737. [CrossRef]
7. Sun, L.M.; Fujino, Y.; Pacheco, B.M.; Chaiseri, P. Modelling of tuned liquid damper (TLD). *J. Wind Eng. Ind. Aerodyn.* **1992**, *43*, 1883–1894. [CrossRef]
8. Wakahara, T.; Ohyama, T.; Fujii, K. Suppression of wind-induced vibration of a tall building using tuned liquid damper. *J. Wind Eng. Ind. Aerodyn.* **1992**, *43*, 1895–1906. [CrossRef]
9. Tamura, Y.; Fujii, K.; Ohtsuki, T.; Wakahara, T.; Kohsaka, R. Effectiveness of tuned liquid dampers under wind excitation. *Eng. Struct.* **1995**, *17*, 609–621. [CrossRef]

10. Sakai, F. Tuned liquid column damper-new type device for suppression of building vibration. In Proceedings of the 1st International Conference on High-Rise Buildings, Najin, China, 1989; pp. 926–931. Available online: https://ci.nii.ac.jp/naid/10007252264 (accessed on 15 March 2020).
11. Colwell, S.; Basu, B. Tuned liquid column dampers in offshore wind turbines for structural control. *Eng. Struct.* **2009**, *31*, 358–368. [CrossRef]
12. Jin, Q.; Li, X.; Sun, N.; Zhou, J.; Guan, J. Experimental and numerical study on tuned liquid dampers for controlling earthquake response of jacket offshore platform. *Mar. Struct.* **2007**, *20*, 238–254. [CrossRef]
13. Chen, B.F.; Yang, B.H. Experimental study of a hybrid TMD and TLD on structure motion reduction. *Ocean Eng.* **2018**, *165*, 538–549. [CrossRef]
14. Veritas, D.N. *Fatigue Design of Offshore Steel Structures*; Det Nor Ske Veritas: Oslo, Norway, 2010.
15. Jonkman, J.; Butterfield, S.; Musial, W.; Scott, G. *Definition of a 5-MW Reference Wind Turbine for Offshore System Development*; National Renewable Energy Lab. (NREL): Golden, CO, USA, 2009.
16. Jonkman, J.; Musial, W. *Offshore Code Comparison Collaboration (OC3) for IEA Wind Task 23 Offshore Wind Technology and Deployment*; National Renewable Energy Lab. (NREL): Golden, CO, USA, 2010.
17. International Electrotechnical Commission. *Wind Turbines—Part 3: Design Requirements for Offshore Wind Turbines*; International Electrotechnical Commission: Geneva, Switzerland, 2009.
18. Standard, O. *Design of Offshore Wind Turbine Structures*; Det Nor Ske Veritas: Oslo, Norway, 2014.
19. International Electrotechnical Commission. *Wind Turbines—Part 1: Design Requirements*; International Electrotechnical Commission: Geneva, Switzerland, 2005.
20. Krabbenhoft, J. Shallow Water Tuned Liquid Dampers. Ph.D. Thesis, Department of Civil Engineering, Technical University of Denmark, Copenhagen, Denmark, 2011.
21. Chen, B.F.; Huang, S.M. A numerical study of liquid tank and structure interaction. *J. Mar. Sci. Technol.* **2015**, *23*, 781–791.
22. Frandsen, J.B. Sloshing motions in excited tanks. *J. Comput. Phys.* **2004**, *196*, 53–87. [CrossRef]
23. Ju, S.H.; Feng-Chien, S.; Yi-Pei, K.; Min-Hsuan, X. Fatigue design of offshore wind turbine jacket-type structures using a parallel scheme. *Renew. Energy* **2018**. [CrossRef]